Implementation of Optical Diagnostics for Study of a Non-Canonical Hypersonic Geometry

Steven J. Beresh,* Anshuman Pandey, Daniel R. Richardson, Douglas W. Carter, Ashley J. Saltzman, and Katya M. Casper

Sandia National Laboratories, Albuquerque, NM, 87185, USA
* Correspondent author: sjberes@sandia.gov

Keywords: Hypersonics, Shock/Boundary-Layer Interaction, Separated Flows, Hypersonic Transition

ABSTRACT

The study of shock/boundary-layer interactions on a non-canonical hypersonic geometry involves physical complexities not found on the canonical investigations that dominate the literature. The present case examines a cone-slice-ramp, which combines an upstream asymmetric flow expansion with a downstream three-dimensional compression ramp. Optical diagnostics of the off-body flowfield are a necessary complement to surface instrumentation including high-frequency pressure sensors and Temperature Sensitive Paint (TSP). Focused Laser Differential Interferometry (FLDI) measured the flowfield distribution of second-mode instability waves responsible for transition. Filtered Rayleigh Scattering (FRS) was used for flow visualization of the separation region and unsteady shear layer. Velocimetry through the separation shear layer was provided by Femtosecond Laser Electronic Excitation Tagging (FLEET) whereas Coherent Anti-Stokes Raman Scattering (CARS) measured the thermal profiles through multiple flow features generated by the interaction. These flowfield diagnostics detail the alterations in the shock/boundary-layer interaction as the flow state moves from laminar to transitional to turbulent conditions, revealing behaviors absent from canonical flows.

1. Introduction

Shock/boundary-layer interactions (SBLI) have been studied for many decades owing to their relevance to external aerodynamics, engine inlets, turbomachinery, and other flight applications. Increased surface heating, unsteady pressure loading, and fluid/structure interactions are the most prominent physical manifestations of SBLI situations (e.g., Dolling [1]). However, the vast majority of these studies, both experimental and computational, have occurred on canonical geometries. These include, as categorized by Refs. [2, 3], impinging shocks, compression ramps, and fins; they may be in planar or axisymmetric configurations and comprise both two-dimensional and swept ramp and fin designs.

Dolling [1] and Gaitonde [3] have noted the limitations of understanding SBLI on realistic geometries by extrapolating from canonical studies, which fits within Smits's broader observation

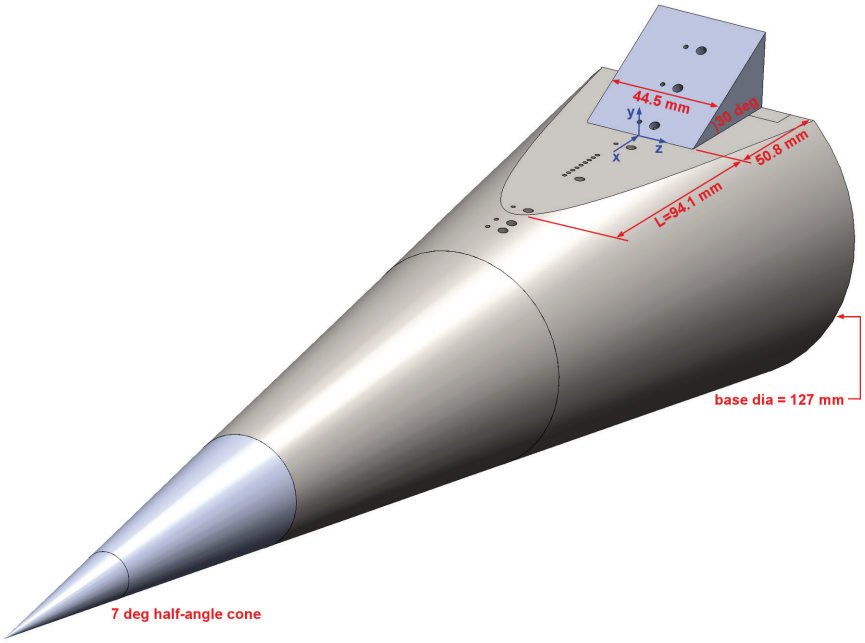

Figure 1. Cone-slice-ramp geometry used in this work and the coordinate system with origin at the midspan of the ramp corner.

that research efforts in wall-bounded flows need to undertake greater complexities than those posed by canonical flows [4]. The community recently has placed greater emphasis on three-dimensional geometries but still largely isolates only a single physical effect in experiments or simulations [5]. Towards this goal, Sandia recently has been studying hypersonic SBLI on a geometry that includes three-dimensional complexities and adds expansion effects upstream of the compression ramp (e.g., [6, 7]). Based on an original concept by Oberkampf and Aeschliman [8], the geometry shown in Figure 1 is a cone-slice-ramp configuration in which a 7-deg half-angle cone is sliced longitudinally parallel to the axis and then a finite-span compression ramp is placed upon it. This design combines the effect of a nonuniform expansion onto the slice with an interchangeable compression ramp of varying angle. Depending upon the wind tunnel Reynolds number, laminar or transitional or turbulent flow may drive the expansion and SBLI.

The flow over the cone-slice-ramp geometry has been studied at Mach 5 and Mach 8 using modern but conventional instrumentation including high-frequency pressure sensors, high-speed schlieren imaging, and Temperature Sensitive Paint (TSP) [6]. The structural response of an embedded flexible panel has been examined as well using accelerometers within the model [9]. Related experiments have been conducted at Purdue University [10, 11]. Continued insight into the flow physics requires not just measurements of surface conditions, but also probing the off-body gas properties to explore the unsteady nature of the separation and reattachment regions. To enable this, laser diagnostics are being implemented including Focused Laser Differential Interferometry

(FLDI), Filtered Rayleigh Scattering (FRS), Femtosecond Laser Electronic Excitation Tagging (FLEET), and Coherent Anti-Stokes Raman Scattering (CARS). The combination of these measurements with surface measurements is exploring the complex physics of SBLI on non-canonical geometries and how they are and are not informed by the body of literature studying canonical SBLI environments.

2. Experimental Apparatus

The Sandia Hypersonic Wind Tunnel (HWT) is a blowdown-to-vacuum facility with interchangeable nozzles and in-line flow heaters for nominal Mach numbers of 5, 8, and 14 [12]. In this report, only the Mach 8 system was used that has a 355.6 mm diameter axisymmetric test section supplied by pure nitrogen. At Mach 8, the stagnation pressure P_0 ranges from 1720-6890 kPa and the stagnation temperature T_0 from 500-890 K, yielding a Reynolds number (*Re*) range from 3.3 − 20 × 10^6 /m. The noise level of the HWT is 3−5%, quantified as the root-mean-square Pitot pressure between 0 to 50 kHz over the mean Pitot pressure [13]. Typical wind tunnel runs lasted approximately 30 seconds.

The wind tunnel model was a 7-deg half-angle sharp cone with a base diameter of 0.127 m on which a horizontal slice has been cut parallel to the cone longitudinal axis, creating a hyperbolic boundary as seen in Fig. 1. A finite-span compression ramp was placed at the aft end of the slice, interchangeable for 0, 10, 20, 30, and 40-deg ramps (where the 0-deg ramp simply maintains the flat slice). The model was mounted using a sting at the base of the cone and all testing was performed at zero angle of attack.

Figure 1 shows numerous sensor holes. The smaller diameter holes mounted Kulite XCQ-062-30A or XCE-062-15A sensors for measuring surface-pressure fluctuations with a 0-50 kHz bandwidth, while the larger holes mounted PCB132B38 sensors that have frequency bandwidth of 11-1000 kHz for high-frequency pressure fluctuations. Additional details are found in [6, 7].

3. Previous Measurements

To capture the unsteadiness in the shock structure and the separated shear layer at the slice-wedge corner, a high-speed schlieren system was used. The light source was an incoherent pulsed diode laser (Cavilux Smart) that generated 10 ns pulses continuously at 100 kHz. The light was passed through a slit to increase sensitivity and then collimated, directed through the test section, and captured and focused onto a knife edge. A high-speed camera (Phantom v2512) equipped with a 105 mm lens then captured the remaining light to produce a schlieren image that captured the density gradients in the flow field. The high-speed laser and camera combination was operated at

100 kHz to provide a picture (640 pixels x 208 pixels) of the unsteady flow over the wedge for 1 second.

As an example of the physical insight that can be provided by combining the pressure sensors with schlieren movies, Fig. 2 shows an average schlieren image annotated with flow features. Pressure sensor locations used for this experiment are shown by the colored dots. This image was acquired at Re=4.5 × 10^6 /m, where the flow is laminar and separation moves far forward to coincide with the expansion corner. The full schlieren movie shows the separation shear layer flapping in time and its reattachment location moving about the surface of the ramp. Pressure sensors on the ramp reveal the frequency content of this behavior. One of these sensors also is plotted in Fig. 2 as Re is raised and the flow becomes transitional and then fully turbulent. A flapping mode of the shear layer is identified at 17 kHz for the laminar and transitional case, but it is absent once the flow becomes turbulent. The high-speed schlieren movies allow for filtering of the data to identify global shear layer behavior associated with this distinct flapping mode, as well as more sophisticated signal analysis such as spectral proper orthogonal decomposition (SPOD) to identify the energy associated with various instabilities as they propagate along the shear layer [14].

A critical feature of this non-canonical geometry also is well identified by the fluctuating pressure measurements. Figure 3 shows pressure fluctuation spectra across the expansion corner but with no compression ramp installed, at Re=5.9 × 10^6 /m. This is a transitional case where second-mode instability waves form along the frustrum of the cone and are strongly present when the flow approaches the expansion corner (x=-107 mm). As the flow progresses past the expansion, the amplitude of the incoming instability wave at about 200 kHz plummets and a new second-mode instability forms at lower frequency in the thicker boundary layer post-expansion (beginning at x= -50 mm). This is due to the relaminarization effect of the expansion, which returns the flow to an earlier state of transition. When a compression ramp is present, this relaminarized boundary layer will be the incoming flow for SBLI.

The relaminarization effect as well as surface heating due to SBLI can be seen in Temperature Sensitive Paint (TSP) data. In these experiments, TSP was accomplished using a Ru(bpy) paint in a clearcoat, excited with 460-nm water-cooled lights. Images were acquired with Lavision sCMOS cameras, high-pass filtered at 550 nm to remove the excitation light. A Schmidt-Boelter heat-transfer gage within the field of view was used for in-situ calibration of the paint to convert the temperature change during a wind tunnel run to heat transfer, nondimensionalized as Stanton Number. The TSP is sufficiently time-resolved to capture changes during a wind tunnel run but not to capture time-dependent flowfield properties.

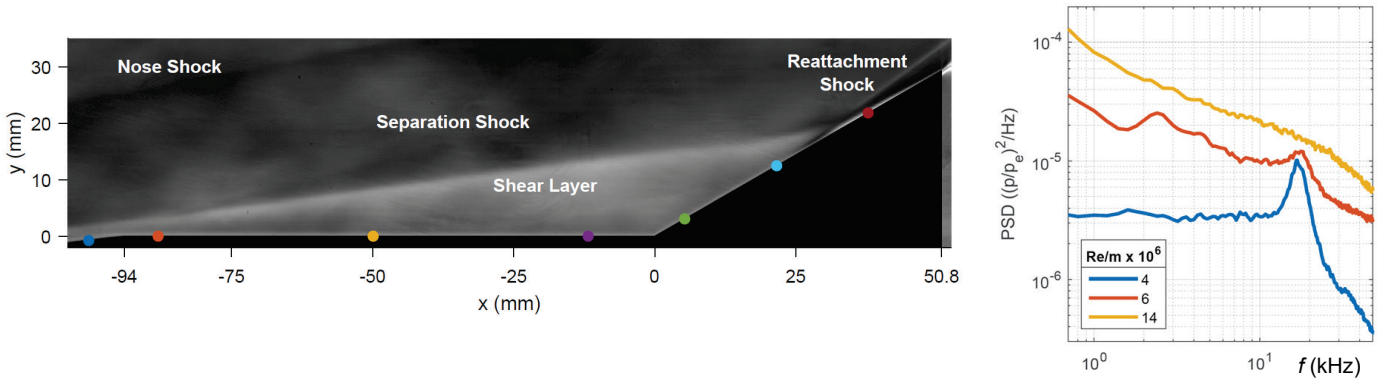

Figure 2. (left) Mean schlieren image of separation and reattachment at Re=4.5 × 10^6 /m; (right) spectra of fluctuating surface pressures within the separation region. Left from [14]; right from [9].

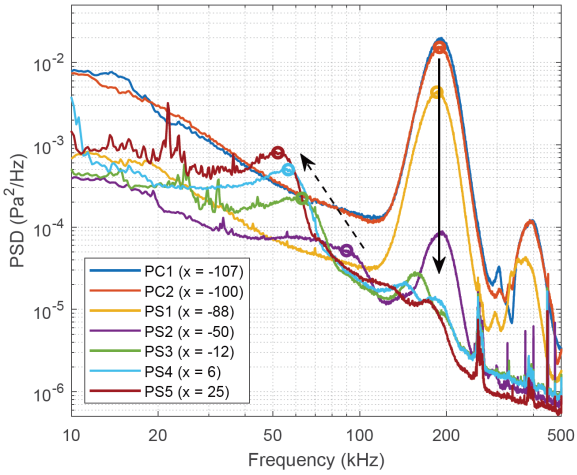

Figure 3. Spectra of pressure fluctuations showing relaminarization effects at Re=5.9×10^6/m. Values of x in mm. From [7].

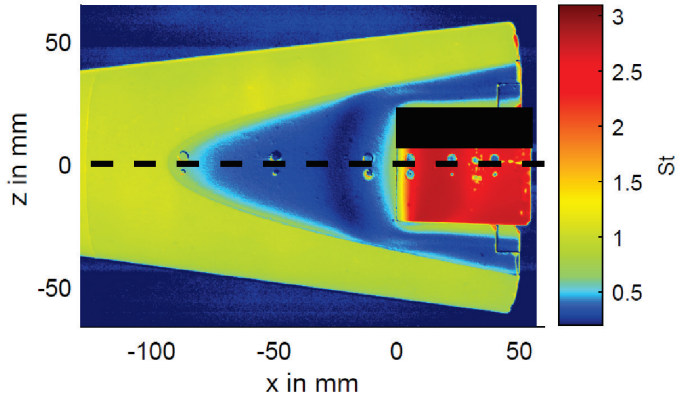

Figure 4. Temperature Sensitive Paint field at Re=12.5×10^6/m, shown in Stanton Number for heat flux. From [6].

Figure 4 shows a TSP field for Re=12.5 × 10^6 /m, a fully turbulent case. Relaminarization still occurs across the expansion corner, as evidenced by the drop in surface heat transfer on the slice, though in this case the flow regresses to a lesser turbulent intensity without becoming laminar. Flow separation near the compression ramp manifests initially as a drop in heat flux (dark blue curved region at about x=-25 mm), then a rise in heat flux nearer the ramp, then finally a much larger increase in heat flux is seen on the compression ramp itself as the flow reattaches. The black band in the image covers a portion of the ramp where no TSP was applied. Flow separation and reattachment locations were verified by schlieren images and surface oil flow tracers.

4. Laser Diagnostics

The complexities of this three-dimensional, non-canonical flow field incorporating both expansion effects and SBLI at a compression corner cannot be fully understood without off-body data. The inherent unsteadiness of the flow field can be captured by flow imaging techniques, and quantitative gas properties are measurable as well. In particular, turbulence quantities involving the fluctuating velocities and temperatures are critical for developing and validating compressible models to enable more accurate simulations.

Particle Image Velocimetry (PIV) is one of the staples of modern fluid dynamics measurements and the Sandia team has much experience using it in high-speed flows. However, PIV has seen only limited deployment in hypersonic testing facilities. This primarily is because even the smallest particles that can be seeded into a flow still exhibit very large particle lag in these low-density, high-velocity-gradient environments. The huge volume flow rates lead to sparse particle densities. Moreover, particle choices that plausibly meet seeding requirements may risk damage to the mechanical systems of most wind tunnels. For these reasons, PIV has not been selected for implementation into HWT.

Owing to its relative ease and affordability, Focused Laser Differential Interferometry (FLDI) recently has become a common tool in hypersonic facilities to detect instability waves. A signal is generated on a photodiode of the interference from a closely-spaced pair of beams focused on the detector. The beam pair generates constructive and destructive interference on the photodiode, subject to aero-optic deflection in the flow by density gradients where the beams are focused [15]. It is capable of measuring frequencies from the kHz range to above 1 MHz, though the spatial resolution of the probe volume becomes poorer at lower frequencies [16]. Frequencies are determined with great accuracy, and although the magnitudes generally are reported as arbitrary units, if the instrument is held stable, they provide relative amplitudes between measurements.

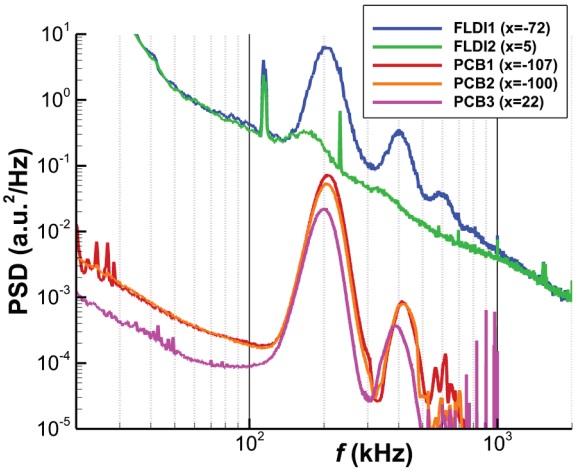

Figure 5. Spectra of FLDI measurements compared to those of pressure fluctuations from PCB surface sensors. From [14].

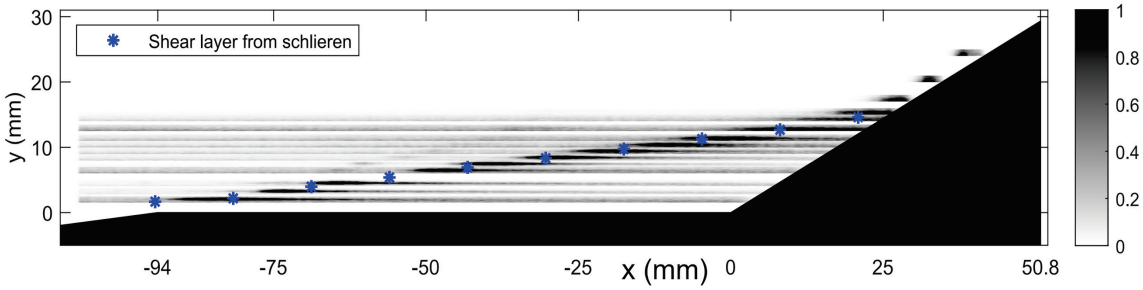

Figure 6. Contours obtained from FLDI intensities in the 130-280 kHz range depicting the separation region at Re=4.5 × 10^6 /m. From [14].

Here, FLDI has been used to measure the second-mode waves within the separation region approaching the compression ramp. Figure 5 shows FLDI measurements at two locations near PCB pressure sensors, about 3 mm above the surface, comparing the instabilities as measured by the fluctuating pressure sensors to those measured by FLDI in the flow field at Re=4.5 × 10^6 /m. The shear layer flapping at the preferred frequency of 17 kHz is not detected because FLDI does not have adequate sensitivity at such relatively low frequencies at which the spatial resolution is poor and some contamination enters from the wind tunnel window boundary layers. The second-mode waves at about 200 kHz are clearly detected by FLDI and match the pressure data. Frequencies match precisely between the two measurement techniques but the amplitudes are in arbitrary units and cannot compare. Several higher harmonics are found as well in the FLDI spectrum from the upstream location. The third and even fourth harmonic can be spotted in the FLDI spectra but they disappear into the noise floor of the pressure spectra. The narrow peak at 115 kHz in the FLDI spectra is due to noise; a harmonic can be observed at 230 kHz as well.

The FLDI beam was scanned horizontally through the separation region at many vertical locations off the wind tunnel model surface. Signals were filtered for the range 130-280 kHz, which contains the second-mode wave energy. These have been mapped onto a spatial grid of the cone-slice-ramp region and normalized by the peak amplitude in this range. The resulting contour is plotted in Fig. 6, which shows a global picture of the separation region that confirms that the second-mode energy predominantly travels along the shear layer as opposed to its near-wall location in the incoming boundary layer. The superposed blue data points represent the mean shear layer position as measured by the high-speed schlieren imaging. The FLDI and schlieren results are very close and therefore portray the picture of second-mode energy propagation coinciding with the shear layer.

A very different optical diagnostic is Filtered Rayleigh Scattering (FRS). FRS functions based on a different physical principle as compared to PIV, relying upon the Doppler shift of narrow linewidth laser light to determine the velocity rather than particle motion (e.g., [17]). This is fairly complex and tedious, using a molecular iodine filter to convert the Doppler-shifted velocity to an imageable intensity and reference it to an unaltered signal. A much simpler approach has proven effective for flow visualization to detect shock waves, turbulent structures, transition instabilities, and shear layers [18]. Conceptually similar to the long-known vapor screen method [19], ethanol or carbon dioxide is evaporated into the wind tunnel test gas well upstream of the nozzle, then the gaseous seed condenses into a fine fog of particles on the order of 10 – 50 nm in diameter. The linewidth of the illuminating laser beam is tuned to a frequency that approximately matches the Doppler-shifted frequency of the flowing gas. Light scattered from the particle fog is passed by an iodine filter, but unshifted light originating from wind tunnel and model surfaces is suppressed. This returns high-quality images that can reveal important fluid dynamic phenomena via instantaneous snapshots and their ensemble averages.

In the present implementation, a liquid carbon dioxide seeder recently was developed for the HWT to create the fog necessary to visualize the flow [20]. It delivers approximately 0.5-1% mass fraction of the HWT flow. An injection-seeded Nd:YAG laser running at 10 Hz provided the narrow-linewidth light at 532 nm and 220 mJ per pulse to scatter off the fog particles, which was collected by an sCMOS camera looking through an iodine filter. The laser sheet was positioned along the centerline of the wind tunnel model. The laser frequency was tuned to absorb background light and pass light at or near the freestream velocity. To obtain the necessary Doppler velocity component, the laser sheet was incident to the test section at an oblique angle to the streamwise direction and the camera could remain normal to the laser sheet.

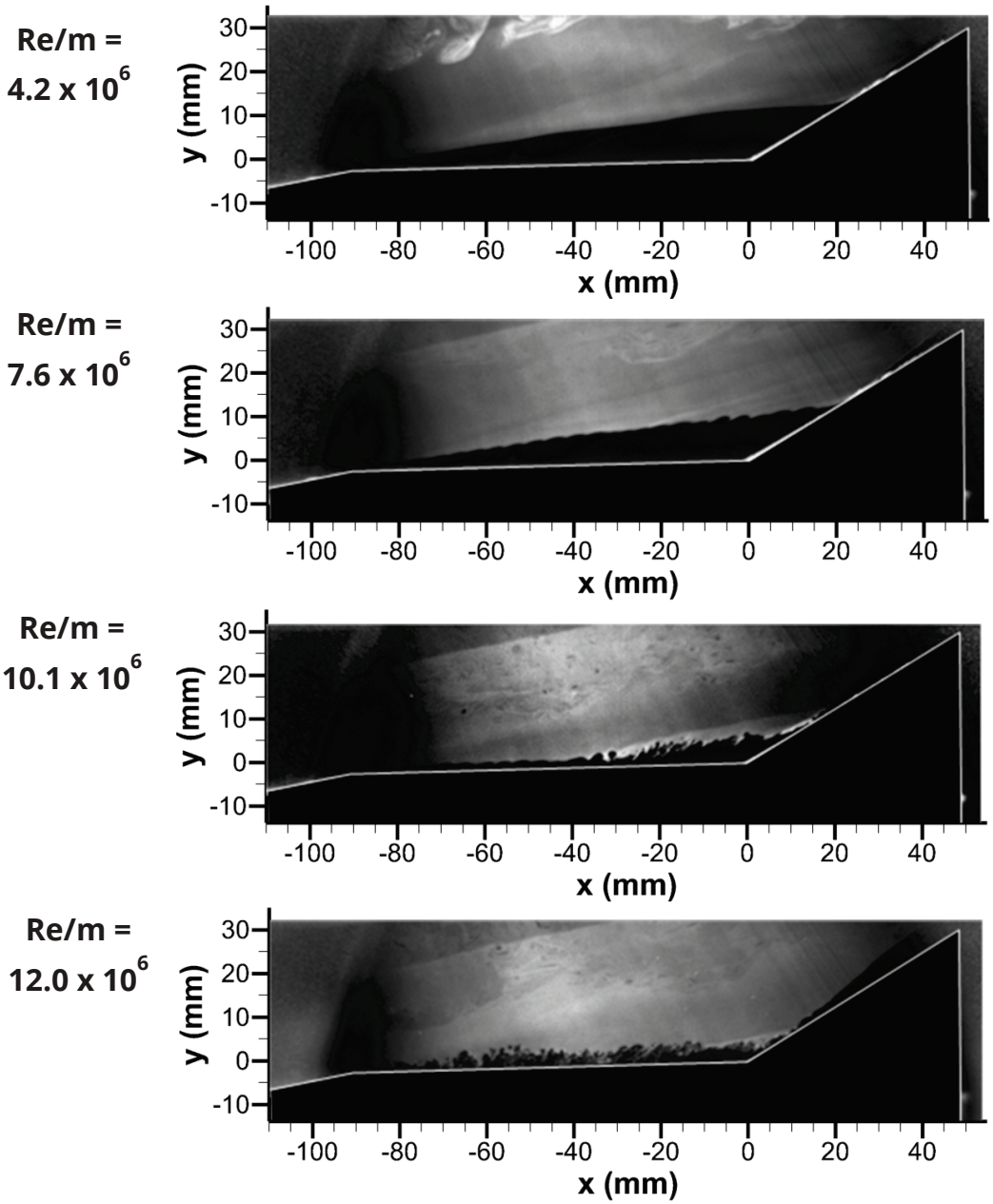

Figure 7. Filtered Rayleigh Scattering instantaneous snapshots of the cone-slice-ramp shock/boundary-layer interaction. From [21].

Sample instantaneous snapshots are shown in Fig. 7. Four images are given at varying Reynolds number that moves the flow from laminar through transitional to turbulent conditions. At *Re*=4.2 × 10^6 /m, flow conditions are laminar and the separation region initiates at the expansion corner with a smooth shear layer interface, though it is known to exhibit some flapping as per Fig. 2. When the Reynolds number is increased to *Re*=7.6 × 10^6 /m, the separation point remains at the expansion corner but the shear layer interface exhibits a structure consistent with second-mode waves. This transition instability appears to propagate along the shear layer rather than near the

surface, which also is what the FLDI measurements demonstrated in Fig. 6. These disturbances have a wavelength of approximately 4 mm, which corresponds to a frequency of about 200 kHz, again consistent with previous data in Fig. 5 using both FLDI and surface pressure sensors. By Re=10.1 × 10^6 /m, the flow is in a late transitional state. Second-mode waves are observed in the boundary layer as it passes over the expansion corner, but then the flow becomes turbulent and the separation point and separation shock move downstream along the slice surface closer to the compression ramp. A higher Reynolds number of Re=12.0 × 10^6 /m leads to a smaller separation region and less prominent separation shock. In all four cases, the reattachment shock can be seen emanating from the ramp surface, though it becomes more prominent with a larger angle for turbulent conditions.

At the present time, velocimetry in HWT is being implemented not by expanding FRS capability, but by developing Femtosecond Laser Electronic Excitation Tagging (FLEET). When illuminated by a femtosecond-time-scale laser, nitrogen fluoresces and points or lines can be written into the flow, whose motion is then tracked in time typically using an intensified camera [22]. Such seedless velocimetry is necessary in hypersonics to avoid the particle lag errors associated with PIV, and the FLEET technique enabled by ultrafast lasers accomplishes such measurements with relative ease compared to older methods that required separate write and read lasers and typically involved toxic gases. The Sandia implementation of FLEET has written beams at the third harmonic (267 nm) for a more Gaussian-shaped fluorescence distribution and negligible deposited energy [23]; pulse energy was about 0.5 mJ. Fluorescent light was collected using an sCMOS camera coupled to an intensifier.

Initial demonstrations of FLEET measured the freestream velocity at Mach 8 and 14 for use in flow characterization and a separate wind tunnel campaign collected velocities in the wake of a sharp cone. The latter is shown in Fig. 8, which displays the mean velocity changes consistent with a shear layer in the wake of the model. A single FLEET line was written into the flow and then imaged using multiple gates on the intensifier. Gaussian distributions were fitted to the line profiles at each transverse position to give sub-pixel resolution of line centers. The long lifetime of the fluorescence allowed several velocity profiles to be obtained from varied gate pairs as the written line convected downstream and eventually decayed. These two demonstrations provided assurance that the FLEET diagnostic was operating as intended and returning viable measurements.

Continued development of the FLEET diagnostic led to a recent implementation on the cone-slice-ramp model. Here, the incident beam must be steered directly at the model, which can produce significant surface damage from energy deposition at femtosecond time scales. To avoid this, three

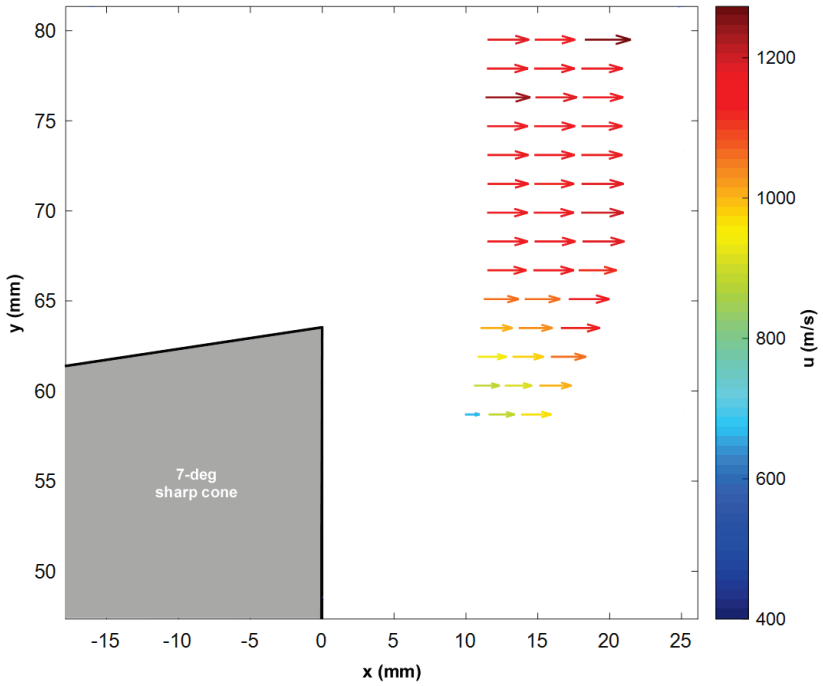

Figure 8. FLEET velocimetry demonstrated at Mach 8 in the HWT of the shear layer in the wake of a sharp cone.

measurement locations were chosen that coincided with the three PCB sensor ports on the slice. The sensors were removed and replaced with seals recessed beneath the surface by 6.5 mm, allowing the beam to terminate without damage to the model and masking any laser flare from the camera. Due to limitations in optical access through the wind tunnel windows suitable for ultrafast beams, the incident beam was pitched a few degrees to enter each sensor port.

Light was collected via two intensifier gates, each 0.3 μs long, with the first delayed from the initial write by a 0.1 μs offset to avoid saturation and the second gate delayed by 2.2 μs from the first. Mean FLEET images were assembled from nearly 1000 individual samples. To improve the signal-to-noise ratio for location of the peaks of the FLEET lines, images were divided into horizontal stripes 32 pixels in height with 50% overlap, each of which was binned into a signal intensity profile. Through trial and error, an autocorrelation method was found to be most robust for extracting peak intensity positions for the present data sets. A gradient-based peak detection located the first peak in the autocorrelation and a three-point Gaussian fit provided sub-pixel accuracy.

A mean FLEET image is shown in Fig. 9a for the downstream sensor location, which is very nearly at the location of the compression corner of the ramp. The flow case is Re=5 × 10^6 /m, at which the separation region extends from the expansion corner across the entire slice. The slightly oblique direction of the FLEET lines is apparent. A small distortion of the line due to the shear layer

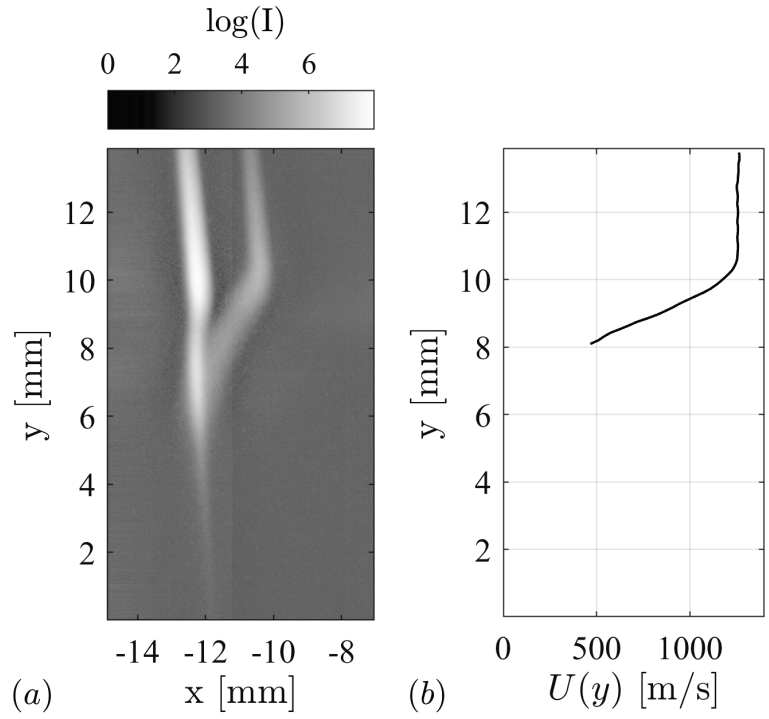

Figure 9. FLEET velocimetry demonstrated near the juncture of the compression ramp for the cone-slice-ramp shock/boundary-layer interaction at Re=5 × 10^6 /m; (a) mean FLEET image showing two detection gates; (b) resulting velocity profile.

is evident in the early first gate, but it is much more pronounced in the second gate. The FLEET line of the second gate is essentially a visual velocity profile of the flow. Once the velocity in the shear layer or the separation region beneath it approaches zero, the two FLEET lines overlap and become difficult to distinguish. At this point, the autocorrelation no longer locates a peak corresponding to the local displacement. Gaussian fitting methods were found ineffective as well. For such small velocities, a more sophisticated interrogation method must be developed, or the problem circumvented using a camera configuration allowing frame-straddling of the two gates. The difficulty is compounded by the low densities in the separation region, which diminish the signal.

Nonetheless, a useful velocity profile is extracted from the FLEET image of Fig. 9a and is shown in Fig. 9b. The FLEET velocities do not resolve below approximately 0.4 u/U_∞ and therefore reverse flow cannot be detected within the separation region. The position of the shear layer is well resolved and its thickness can be inferred from the velocity profile shape. Figure 9 demonstrates the essential success of measuring velocities in this complex hypersonic environment. Data at additional Re and all three sensor locations are forthcoming [24].

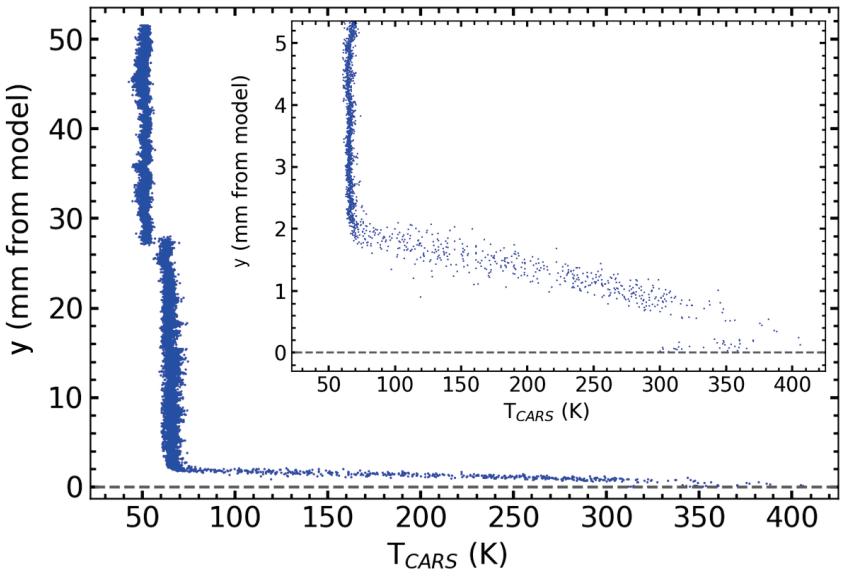

Figure 10. CARS temperature measurements of the thermal boundary layer on a sharp cone at Mach 8, located 420 mm from the nose.

Finally, Coherent Anti-Stokes Raman Scattering (CARS) has been implemented in the HWT to measure the gas temperature. The Sandia system is a hybrid CARS approach that generates a pump beam from a femtosecond laser and a probe beam from a pulse-stretched picosecond beam formed from a portion of the frequency-doubled femtosecond source [25]. As opposed to a nanosecond CARS system, the hybrid system pumps many ro-vibrational transitions to provide much improved sensitivity in the cold, low-pressure nitrogen test gas in HWT. A short probe delay for temperature measurements nearly eliminates the gas-phase molecular collisions that may alter the Raman coherence. The femtosecond laser operates at a 1 kHz repetition rate with 3 mJ per pulse.

Like the initial phases of FLEET implementation, CARS first was conducted in the wind tunnel freestream at Mach 8 and 14 to better characterize the flow conditions of the nozzle expansion [26] and compare to conventional measurements using thermocouple probe rakes. These tests were used to solve challenges associated with the low-temperature, low-density hypersonic environment, which are not the natural operating conditions for CARS. Following validation of a successful measurement capability, the diagnostic was applied to the thin boundary layer of a sharp cone at Mach 8, shown in Fig. 10 at a location 420 mm axially downstream of the cone tip. The CARS probe volume and collection optics were translated normal to the model central axis during the course of a wind tunnel run to obtain the profile. The thermal boundary layer is revealed with impressive precision and spatial resolution, demonstrating the capability of the CARS system in

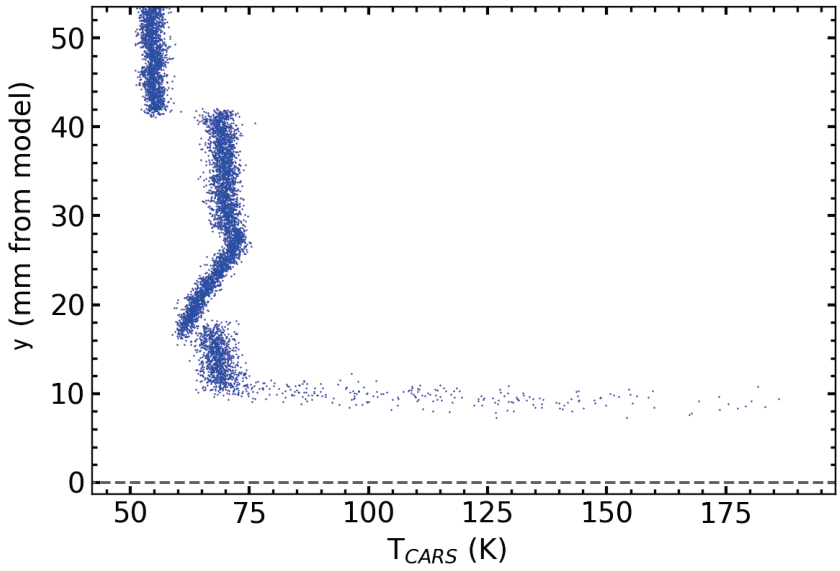

Figure 11. CARS temperature measurements of the thermal profile located at the juncture of the compression ramp for the cone-slice-ramp shock/boundary-layer interaction at Re=6.5 × 10^6 /m.

HWT. Even the peak temperature is discerned only 0.2 - 0.4 mm from the cone surface before turning back down towards the cooler wall temperature (initially at ambient room temperature).

Subsequently, measurements were collected at multiple stations along the cone-slice-ramp model roughly corresponding to the PCB sensor locations along the slice. Several values of Re were tested as well. Figure 11 provides the thermal profile normal to the slice at the junction with the compression ramp at Re=6.5 × 10^6 /m. Passage of the bow shock from the nosetip is observed via a temperature jump at approximately z=42 mm. Between that location and the surface, the complexity of the temperature profile can be provisionally understood in the context established by earlier diagnostics. The large temperature rise occurring at about z=10 mm and increasing towards the surface is due to the separation shear layer; this location is confirmed by the schlieren of Fig. 2 and the FLDI of Fig. 6. The CARS signal then deteriorates closer to the wall and continued measurement is not possible. It is not yet understood whether this is due to decreasing density in the separation region or aero-optical effects from strong turbulent fluctuations that interfere with the CARS beam overlap. The magnitude of the temperature profile decreases towards the wall in the range z=16-26 mm likely owing to expansion waves from the cone-slice corner, whereas the small but sharp jump at z=16 mm probably is created by the separation shock. The FRS images in Fig. 7, though not quite matching the Re of Fig. 11, support this supposition. More scrutiny of all the diagnostics in totality is warranted to fully appreciate the nature of the temperature profile. Meanwhile, temperature profiles were acquired at multiple Re and measurement stations and will be fully reported in a forthcoming publication [27].

5. Conclusion

The study of shock/boundary-layer interactions (SBLI) on a non-canonical geometry involves physical complexities not found on the canonical investigations that dominate the literature. This challenge is enhanced when the strong compressibility effects of hypersonic flow are present as well. To gain a satisfactory understanding of the challenging fluid dynamics, optical diagnostics of the off-body flowfield are necessary as a complement to surface instrumentation.

In the present case, a cone-slice-ramp was selected as the non-canonical geometry to study, which combines an upstream asymmetric flow expansion with a downstream three-dimensional compression ramp. High-frequency pressure sensors have been employed for many years on the surface of this wind tunnel model, with Temperature Sensitive Paint (TSP) used to derive the mean surface heat flux and high-frame-rate schlieren imaging to record the dynamics of shock waves and the separation shear layer. The present work adds laser-based flow diagnostics for further insight. Focused Laser Differential Interferometry (FLDI) was used to measure the flowfield distribution of second-mode instability waves responsible for transition. Filtered Rayleigh Scattering (FRS) was used for flow visualization of the separation region and unsteady shear layer, and it also revealed the propagation of incoming boundary layer instability waves. Velocimetry was provided by Femtosecond Laser Electronic Excitation Tagging (FLEET), revealing the position and shape of the shear layer bounding the separation region of the SBLI. Coherent Anti-Stokes Raman Scattering (CARS) measured the thermal profile through multiple flow features generated by the SBLI, building on a demonstrated success measuring the thermal boundary layer profile. These flowfield diagnostics are detailing the alterations in the shock/boundary-layer interaction on a three-dimensional geometry as the flow state moves from laminar to transitional to turbulent conditions, revealing behaviors not present in canonical flows.

Acknowledgments

The authors thank Rajkumar Bhakta, Brian Denk, Marie de Zetter, J. Clark Pehrson, and Russell Spillers for their contributions to operating the wind tunnel and instrumentation, as well as Yibin Zhang for an earlier phase of FLEET development.

Sandia National Laboratories is a multi-mission laboratory managed and operated by National Technology and Engineering Solutions of Sandia, LLC., a wholly owned subsidiary of Honeywell International, Inc., for the U.S. Department of Energy's National Nuclear Security Administration under contract DE-NA0003525.

References

[1] Dolling, D., "Fifty Years of Shock-Wave/Boundary-Layer Interaction Research: What Next?," *AIAA Journal*, Vol. 39, No. 8, 2001, pp. 1517-1531.

[2] Clemens, N. T., and Narayanaswamy, V., "Low-Frequency Unsteadiness of Shock Wave/Turbulent Boundary Layer Interactions," *Annual Review of Fluid Mechanics*, Vol. 46, 2014, pp. 469-492.

[3] Gaitonde, D. V., "Progress in Shock Wave/Boundary Layer Interactions," *Progress in Aerospace Sciences*, Vol. 72, 2015, pp. 80-99.

[4] Smits, A. J., "Some Observations on Reynolds Number Scaling in Wall-Bounded Flows," *Physical Review Fluids*, Vol. 5, 2020, pp. 110514.

[5] Gaitonde, D. V., and Adler, M. C., "Dynamics of Three-Dimensional Shock-Wave/Boundary Layer Interactions," *Annual Review of Fluid Mechanics*, Vol. 55, 2023, pp. 291-321.

[6] Pandey, A., Casper, K. M., Spillers, R. W., Soehnel, M., and Spitzer, S., "Hypersonic Shock Wave – Boundary-Layer Interaction on the Control Surface of a Slender Cone," AIAA Paper 2020-0815, January 2020.

[7] Pandey, A., Casper, K. M., and Beresh, S. J., "Relaminarization Effects in Hypersonic Flow on a Three-Dimensional Expansion-Compression Geometry," *Journal of Fluid Mechanics*, Vol. 985, 2024, pp. A25.

[8] Oberkampf, W. L., and Aeschliman, D. P., "Joint Computational/Experimental Aerodynamics Research on a Hypersonic Vehicle. Part 1: Experimental Results," *AIAA Journal*, Vol. 30, No. 8, 1992, pp. 2000-2009.

[9] Pandey, A., Casper, K. M., Beresh, S. J., Bhakta, R., and Spillers, R., "Hypersonic Fluid-Structure Interaction on a Cone-Slice-Ramp Geometry," *AIAA Journal*, Vol. 61, No. 5, 2023, pp. 2217-2233.

[10] McKiernan, G. R., and Schneider, S. P., "Instability and Transition on a Cone with a Slice and Ramp at Mach 6," AIAA Paper 2021-0249, January 2021.

[11] Francis, A. A., Dylewicz, K., Klothakis, A., Theofilis, V., and Jewell, J. S., "Instability Measurements on a Cone-Slice-Flap in Mach 6 Quiet Flow," AIAA Paper 2024-0500, January 2024.

[12] Beresh, S. J., Casper, K. M., Wagner, J. L., Henfling, J. F., Spillers, R. W., Pruett, B. O. M., "Modernization of Sandia's Hypersonic Wind Tunnel," AIAA Paper 2015-1338, January 2015.

[13] Casper, K. M., Beresh, S. J., Henfling, J. F., Spillers, R. W., Pruett, B. O. M., and Schneider, S. P., "Hypersonic Wind Tunnel Measurements of Boundary-Layer Transition on a Slender Cone," *AIAA Journal*, Vol. 54, No. 4, 2016, pp. 1250-1263.

[14] Pandey, A., Casper, K. M., Guildenbecher, D. R., Beresh, S. J., Bhakta, R., DeZetter, M. E., and Spillers, R., "Instability Measurements in Hypersonic Flow on a Three-Dimensional Cone-Slice-Ramp Geometry," AIAA Paper 2022-1578, January 2022.

[15] Parziale, N. J., Shepherd, J. E., and Hornung, H. G., "Differential Interferometric Measurement of Instability in a Hypervelocity Boundary Layer," *AIAA Journal*, Vol. 51, No. 3, 2013, pp. 750-753.

[16] Lawson, J. M., Neet, M. C., Grossman, I. J., and Austin, J. M., "Static and Dynamic Characterization of a Focused Laser Differential Interferometer," *Experiments in Fluids*, Vol. 61, 2020, pp. 187.

[17] Elliott, G. S., and Beutner, T. J., "Molecular Filter Based Planar Doppler Velocimetry," *Progress in Aerospace Sciences*, Vol. 35, 1999, pp. 799-845.

[18] Poggie, J., Erbland, P. J., Smits, A. J., and Miles, R. B., "Quantitative Visualization of Compressible Turbulent Shear Flows using Condensate-Enhanced Rayleigh Scattering," *Experiments in Fluids*, Vol. 37, 2004, pp. 438-454.

[19] McGregor, I., "The Vapour-Screen Method of Flow Visualization," *Journal of Fluid Mechanics*, Vol. 11, 1961, pp. 481-511.

[20] Saltzman, A. J., Beresh, S. J., Casper, K. M., Denk, B. P., Bhakta, R., De Zetter, M. E., and Spillers, R. W., "Carbon Dioxide Seeding System for Enhanced Rayleigh Scattering in Sandia's Hypersonic Wind Tunnel," AIAA Paper 2022-4131, June 2021.

[21] Saltzman, A. J., Pandey, A., Beresh, S. J., Casper, K. M., Bhakta, R., Denk, B. P., De Zetter, M. E., and Spillers, R. W., "CO2-Enhanced Filtered Rayleigh Scattering for Study of a Hypersonic Cone-Slice-Ramp Geometry," AIAA Paper 2023-1371, January 2023.

[22] Danehy, P. M., Burns, R. A., Reese, D. T., Retter, J. E., and Kearney, S. P., "FLEET Velocimetry for Aerodynamics," *Annual Review of Fluid Mechanics*, Vol. 54, 2022, pp. 525-553.

[23] Zhang, Y., Beresh, S. J., Casper, K. M., Richardson, D. R., Soehnel, M. M., and Spillers, R. W., "Tailoring FLEET for Cold Hypersonic Flows," AIAA Paper 2020-1020, January 2020.

[24] Carter, D. W., Pehrson, J. C., Bhakta, R., Spillers, R. W., and Beresh, S. J., "Hypersonic FLEET Velocimetry on a Three-Dimensional Expansion-Compression Geometry," to be presented at the 2025 AIAA Science and Technology Forum, January 2025.

[25] Kearney, S. P., and Scoglietti, D.J., "Hybrid Femtosecond/Picosecond Rotational Coherent Anti-Stokes Raman Scattering at Flame Temperatures using a Second-Harmonic Bandwidth-Compressed Probe," *Optics Letters*, Vol. 38, No. 6, 2013, pp. 833-835.

[26] Richardson, D. R., Kearney, S. P., and Beresh, S. J., "Gas-Phase Temperature Measurements in a Mach 8 and 14 Cold-Flow Hypersonic Wind Tunnel via Femtosecond Coherent Anti-Stokes Raman Spectroscopy," AIAA Paper 2024-2321, January 2024.

[27] Richardson, D. R., Ketchum, R. S., Kearney, S. P., and Beresh, S. J., "Hypersonic Thermal Boundary Layer Profiles in a Mach 8 Cold-Flow Hypersonic Wind Tunnel via Femtosecond Coherent Anti-Stokes Raman Spectroscopy," to be presented at the 2025 AIAA Science and Technology Forum, January 2025.